Low-degree convection with melting and application to the Martian northern hemisphere

by

P. James Dennedy-Frank

Submitted to the Department of Earth, Atmospheric, and Planetary Sciences
in partial fulfillment of the requirements for the degree of

Master of Science in Earth and Planetary Sciences

at the

MASSACHUSETTS INSTITUTE OF TECHNOLOGY

September 2006

Author .....
Department of Earth, Atmospheric, and Planetary Sciences
August 16, 2006

Certified by .....
Maria T. Zuber
E.A. Griswold Professor of Geophysics
Thesis Supervisor

Accepted by .....
Maria T. Zuber
E.A. Griswold Professor of Geophysics
Chair, Department of Earth, Atmospheric, and Planetary Sciences

Low-degree convection with melting and application to the Martian northern hemisphere

by

P. James Dennedy-Frank

Submitted to the Department of Earth, Atmospheric, and Planetary Sciences
on August 16, 2006, in partial fulfillment of the
requirements for the degree of
Master of Science in Planetary Science

Abstract

I investigate the hypothesis that the young and smooth surface of the Martian northern hemisphere is due to volcanic resurfacing driven by degree-one convection. I implement a batch melting process in a finite element convection model and run numerical experiments to quantify the melt fraction, timing of melting, and timing of the onset of degree-one convection. All models include a stratified viscosity to induce degree-one flow. To assure that the model's result is robust I vary the model's initial conditions, core-mantle boundary temperature and radius, and the thickness of the lithospheric lid. Long-wavelength convection is a consistent result of the viscosity stratification, and degree-one occurs in one third of the numerical experiments. I compare the melt fraction and onset of degree-one convection to the geological evidence from Martian orbiters, rovers, and meteorites. Good agreement is found between the numerical models and geological evidence, so this model suggests that volcanism driven by degree-one convection may play a significant role in the young age of the northern hemisphere of Mars.

Thesis Supervisor: Maria T. Zuber
Title: E.A. Griswold Professor of Geophysics

Acknowledgments

Writing a thesis, like living life in general, is only done with the help of others. I would like to thank all those who helped me along the way, though I will undoubtedly forget someone; my apologies to all those for whom I lack sufficient space on the paper or in my memory right now.

Advisors are an important part of the graduate school experience, both for the technical and personal aspects. Maria Zuber provided the idea for this project as well as the funding. She let me search for the answers, and I am better for it. Bradford Hager served as my primary contact for any science questions; his off-the-cuff remarks often clarified the important fluid dynamics at work, and I learned a great deal in our talks. For grounding my thought in petrological data and teaching me everything I know about melting, Tim Grove has my thanks. He also served as a good running partner. Rick Binzel supported me through hard times and always had a kind word to boost my ego, for which I will always be grateful. He also gave me my first chance to teach, and served as a great model as a professor. Shijie Zhong provided technical help with the CITCOM code and was incredibly responsive to my many requests for clarification or tests. Finally, Mark Simons had no direct role in this project, but introduced me to the world of planetary geophysics and has always given me good advice.

The lifeblood of the EAPS department is its students, and too many of them have been a significant part of my life to name all of them here. The first recognition goes to "original" residents of 521–it was a really great office. Chin-Wu Chen and I shared many late nights, but he always kept good cheer. On our many walks and coffee stops, Sarah Stewart Johnsonwas my moral support, always believing in me and going to great lengths to show it. Erwan Mazarico served as a sounding board when I was stuck on a problem, and we usually figured it out together. Serving also as my 610 office-mate, Einat Lev, discussed the finer points of fluid dynamics and finite element codes with me, as well as the issues of minorities in science and the conflicts in Israel. Through it all she became a good friend, there when I needed

someone to help me see my way through life. I will miss going to Mass with Maureen Long on Sunday evenings, along with all the Boston Red Sox talk. The petrologists Jay Barr, Anna Monders, Etienne Médard, and Mike Krawczynski clarified the murk when questions of melting came up and also were great folk with whom to run, walk, watch baseball, and eat cookies. For many science discussions and fun times, I would also like to thank Wes Watters, Doug Jerolmack, Scott Lundin, Kristen Cook, and Emily Van Ark.

Of course, life also goes on outside of the office, and many of life's most important times happen there. I want to thank those with whom I had fun and learned about life. Hector Hernandez taught me a great deal about being latino and inspired me to make a meaningful difference. Many MITOCers went on adventures with me, particularly Chris Studnicki-Gizbert, Max Cohen, Dan Walker, Rick Abbott, Anne Lightbody, Paulina Varshavskaya, Natalia Hernandez-Gardiol, and Kristin Mattern. A special thanks to Justin Fitzpatrick, my main climbing partner, who tied his life to mine, both literally and figuratively. Old friends are always welcome in a new place, and Mike Russo gave me a good introduction to Boston my first year here. Lara Rogers and Angela Wilcox were both special people in my life, and I wish them both the best. Finally, but in no way least, thanks to my brother Daniel and parents David and Diane, who have been there to cheer me on, cheer me up, and remind me just to hold on.

Contents

List of Figures

List of Tables

Chapter 1

The Mars dichotomy: Differences between hemispheres

The earliest spacecraft to explore Mars imaged only the Southern Hemisphere and returned images reminiscent of the lunar highlands: an ancient, heavily cratered surface disturbed mainly by impacts since crustal formation. The Mariner 9 mission, the first to pass over Mars' Northern Hemisphere, forced a reevaluation of Mars' geological history. Its images showed a smooth surface with very few craters, interpreted as a much younger surface, in the Northern Hemisphere (*Hartmann*, 1973). Since this asymmetry is of planetary scale, it likely provides clues to the thermal evolution of Mars, and has been the topic of much work and speculation. Theories proposed to explain the differences between the Northern and Southern Hemisphere of Mars include: a massive impact in the Northern Hemisphere (*Wilhelms and Squyres*, 1984), an early episode of plate tectonics (*Sleep*, 1994), and a magma ocean that overturned due to an unstable density structure (*Elkins-Tanton et al.*, 2003). None of these hypotheses are completely consistent with the observations, so the dichotomy between the North and South on Mars remains an interesting phenomenon to study.

1.1 Dichotomy: Measures and models

1.1.1 Dichotomy measurements

The differences between the Northern and Southern Hemispheres on Mars are commonly referred to as the hemispheric dichotomy, crustal dichotomy, or with similar terms. However, several physical properties exhibit a dichotomy between North and South; the origin of the differences may be distinct for each physical property. Perhaps most fundamental and of the earliest origin are the differences in topography and crustal thickness. The Northern Hemisphere is about 6 km lower than the Southern Hemisphere (*Smith et al.*, 1999), and the crust is about 25 km thicker in the South (an average 35 km thick in the North versus an average 60 km thick in the South) (*Neumann et al.*, 2004; *Esposito et al.*, 1992; *Solomon et al.*, 2005). The timing and mechanism of the origin of these differences have been investigated, though few constraints exist. *Phillips et al.* (2001) show that the dichotomy in topography must have existed early in Mars history, since Noachian-age (~4.5-3.8 Ga) channels go downhill from the Southern Hemisphere to the Northern Hemisphere, suggesting that a topographic gradient already existed. Furthermore, *Frey et al.* (2002) suggest that a Noachian surface underlies the current Hesperian-age (~3.8-3.1 Ga) Northern Hemisphere surface. No plausible mechanism could reduce the crustal thickness without disturbing this older surface or destroying the Noachian-aged channels.

The initial observations of Mars' surface consisted of images, so the first differences observed between North and South were smoothness (*Hartmann*, 1973; *Kreslavsky and Head.*, 2000) and age (*Hartmann*, 1973; *Frey et al.*, 2002). The smooth Northern Hemisphere has often been explained by the presence of an early Martian ocean (*Parker et al.*, 1989; *Head et al.*, 1999), although the evidence for this is controversial and complicated by the presence of multiple possible shorelines (*Head et al.*, 1999; *Carr and Head*, 2003). Alternatively, *Tanaka et al.* (2003) suggest that deposition of sediment by outflow channels followed by permafrost processes could smooth the Northern Hemisphere. Counting of observable craters using assumptions of impactor flux has established the Northern Hemisphere age as Early Hesperian to Hesperian;

in contrast, the Southern Hemisphere has a surface of Noachian age. As noted above, recent work has shown that the topography differences existed early (*Phillips et al.*, 2001) and that underlying the Early Hesperian surface is crust of Noachian age (*Frey et al.*, 2002). As a result, models consistent with the data must preferentially resurface a low, old, thin-crusted Northern Hemisphere in the Early Hesperian .

In addition to the physiographic differences, measurements suggest that a petrological difference also exists between the surfaces of the Northern and Southern Hemispheres of Mars. Analysis of data from the Thermal Emission Spectrometer (TES) (*Bandfield et al.*, 2000) groups the non-dust spectral data into two types, one found preferentially in the Southern Hemisphere, the other in the Northern Hemisphere. *Bandfield et al.* (2000) claim that the Type I spectral signal in the Southern Hemisphere corresponds to a basaltic composition, mostly clinopyroxene and plagioclase, while the Type II Northern Hemisphere signal matches spectra of plagioclase and volcanic glass-rich andesite. The source of the Type II spectra has been the topic of much debate, however; *Wyatt and McSween* (2002) suggest that spectra for a weathered basalt fit the data in the Northern Hemisphere equally well. Recent measurements from the visible-infrared spectrometer OMEGA aboard Mars Express (*Bibring et al.*, 2005; *Mustard et al.*, 2005) show that the Type I regions are rich in high-calcium pyroxenes, and that low-calcium pyroxenes are common in Noachian terrains. The Northern Hemisphere plains do not exhibit visible-infrared spectra typical of largely crystalline igneous minerals, which might suggest that weathering broke down such products; however, they do not show significant amounts of hydrated phases, so it seems unlikely they were created via weathering by water. The presence of olivine in craters in the Northern Hemisphere further argues against significant aqueous alteration. These compositional differences suggest that either the Northern and Southern Hemisphere surfaces have distinct petrogenetic origins, or the Northern Hemisphere surface was altered after emplacement.

Finally, there is an asymmetry in the crustal remnant magnetic field, with much stronger magnetic sources in the South. *Connerney et al.* (1999) suggest that this asymmetry is due to a plate tectonics mode with oceanic crust getting "trapped"

in the Southern Hemisphere. The Northern Hemisphere might not show magnetic striping similar to that in Earth's oceans due to the insulation of magnetic sources with non-magnetic cover, hydrothermal alteration of magnetic minerals, or impact demagnetization (*Connerney et al.*, 2005).

1.1.2 Dichotomy models

Many models have been used to replicate the significant differences between the Northern and Southern Hemispheres on Mars. *Sleep* (1994) suggests that a plate tectonics process with mid-ocean ridge-like spreading in the Northern Hemisphere provides an explanation for the crustal thickness, age, and topography asymmetries that is consistent with the large-scale heat-loss process on Earth. However, the gravity field and geologic structures of Mars do not show the subduction zone features or age progression indicative of plate tectonics. In addition, the presence of a Noachian crust beneath the current Early Hesperian surface means that any plate tectonics episode must have been short-lived. *Wilhelms and Squyres* (1984) claim that the difference in crustal thickness and topography could be caused by an extremely large impact in the Northern Hemisphere, based on the presence of low topography and suggestive images from the Viking missions. Gravity data from the MGS mission does not show the signature expected from such an impact (*Zuber et al.*, 2000), nor is this hypothesis consistent with evidence of a Noachian crust (*Frey et al.*, 2002); in addition, the Northern Plains are not roughly circular, as would be expected from an impact. Other researchers (e.g., *Hartmann* (1973)) have proposed that many large impacts in the Northern Hemisphere could create the dichotomy in topography, but it is unlikely such an asymmetry between the number of impactors in the two hemispheres would have occurred; also, the topography and gravity data do not show signs of such impacts except for the Utopia basin (*Zuber et al.*, 2000). *Zhong and Zuber* (2001) propose that degree-one convective flow (convection with a single large upwelling and an antipodal downwelling, a velocity distribution that has most of its power in spherical harmonic degree one) provides an endogenous explanation of the topography, crustal thickness, and age differences. They use analytical and numerical models to show

that a variation in viscosity with depth, specifically a low-viscosity upper mantle, leads to degree-one flow. They suggest that such a viscosity structure is likely given our knowledge of the viscosity structure of the Earth (*Hager and Richards*, 1989) and the temperature- and pressure-dependence of rock rheology. In their work, however, a degree-one convection cell requires hundreds of millions of years to form, inconsistent with the current knowledge of an early low surface on Mars (*Phillips et al.*, 2001; *Frey et al.*, 2002). Based on the model of *Zhong and Zuber* (2001), degree-one convection cannot form the hemispheric dichotomy in topography or crustal thickness, but this does not rule out degree-one flow and associated volcanism as the source of age and composition differences between the hemispheres. Recent work by *Roberts and Zhong* (2006) shows that three-dimensional models with temperature- and pressure-dependent viscosity allow for the rapid onset of a degree-one convective planform, and work on this hypothesis is ongoing. Alternatively, *Elkins-Tanton et al.* (2003) raise the idea that Mars had a magma ocean that led to global mantle overturn after an unstable density structure formed by crystallization of the magma ocean from the bottom. This process could create the dichotomy in topography and crustal thickness very early in Martian history, consistent with current knowledge, but does not address the young age of the Northern Hemisphere surface. The smoothness and young age of the Northern Hemisphere could be modifications by later processes.

1.2 Resurfacing of Northern Hemisphere

Data from the Mars Orbiter Laser Altimeter (MOLA) (*Smith et al.*, 1999), and particularly work by *Frey et al.* (2002), shows that the Early Hesperian Northern Hemisphere surface overlies a Noachian surface. This stratigraphic relationship suggests that filling material from some process must have covered the Noachian Northern Hemisphere without significantly disrupting the earlier surface. The two obvious candidates for such a process are volcanism and sedimentation. I estimate the total thickness of fill in the Northern Hemisphere by calculating the total volume of the Noachian craters in the Northern Hemisphere with diameters from $50\,km$ to $500\,km$,

as shown in *Frey et al.* (2002). This calculation shows that filling these craters requires $3 * 10^5\ km^3$ of material, corresponding to a $300\ m$ average fill thickness over the Northern Hemisphere. *Head et al.* (2002) use MOLA topography of regions in Noachis Terra and Terra Tyrrhena (Early to Middle Noachian units near the topography dichotomy boundary) to examine the morphology that would exist if they were filled with volcanic deposits to an equipotential surface (a first-order estimate of the distribution due to very low-viscosity and diffuse-sourced volcanism). They suggest that $900\ m$ of average fill thickness results in a morphology that resembles Northern Hemisphere units where Noachian material seems to peek out beneath the Early Hesperian surface.

Both volcanic and sedimentary resurfacing of the Northern Hemisphere have been studied. *Hynek and Phillips* (2001) map the eroded surfaces of Arabia Terra and Margaritifer Sinus, and estimate that the volume of material eroded would provide only $120\ m$ of fill thickness throughout the Northern Hemisphere. Although the remaining fill could come from erosion on other parts of Mars, the work of *Hynek and Phillips* (2001) examines the most clearly eroded areas on Mars. As noted in section 1.1.1, previous work suggests that much of the Northern Hemisphere is covered by volcanic flows of Hesperian age (*Scott and Tanaka*, 1986; *Greeley and Guest*, 1987; *Tanaka and Scott*, 1987; *Tanaka et al.*, 1992). More recently, *Head et al.* (2002) propose that deformation of Hesperian volcanic flows by the stress of the Tharsis load best explains a series of wrinkle-ridges circumferential to Tharsis which are not visible in images but which are revealed by mid-range filtering of MOLA topography.

Based on this previous work, I believe it is unlikely that sediments provide all of the fill material in the Northern Hemisphere, and suggest that volcanic resurfacing accounts for a significant portion of the Northern plains. There are two possible mechanisms for localizing such a large volume of volcanic outflow in a single hemisphere. This single-hemisphere volcanism could correspond to planet-wide upwelling moderated by the dichotomy in crustal thickness; future work should examine this possibility. Here I investigate the second possibility, that degree-one convection leads to decompression melting in the upwelling hemisphere, resulting in volcanism in a

single hemisphere.

1.3 The degree-one convection hypothesis

Degree-one convection has been invoked to explain both the Tharsis volcanic zone (*Harder and Christensen*, 1996; *Breuer et al.*, 1998) and the topographic, crustal thickness, and age dichotomies on Mars (*Zhong and Zuber*, 2001; *Roberts and Zhong*, 2006). Degree-one convection develops in a planet with the core size and planetary radius of Mars when a variation in physical properties with depth, such as a mineralogical phase change or temperature- and pressure-dependent viscosity, drives a long-wavelength perturbation to be the fastest-growing structure in the lower mantle. The upper mantle ("weaker" than the lower in the appropriate property) is forced into degree-one flow. *Zhong and Zuber* (2001) use a Rayleigh-Taylor instability analysis and finite element convection models to examine the development of degree-one convection when viscosity varies with temperature and pressure, resulting in a weak upper mantle. Studies that suggest that the Earth's viscosity increases in the lower mantle (*Hager and Richards*, 1989; *Simons and Hager*, 1997) and knowledge of the temperature and pressure dependence of viscosity in mantle rocks (*Karato and Wu*, 1993) motivate such a model. *Roberts and Zhong* (2006) extend such studies to three-dimensional geometries and verify the development of a degree-one convective planform under these conditions. *Harder and Christensen* (1996) note that the Martian core-mantle boundary may occur around the pressure of the γ-spinel to perovskite phase transition, and use a finite element model with an endothermic phase change in the lowermost mantle to develop degree-one convection. However, such a model requires about 2 Ga to develop a single upwelling, too slow for resurfacing the Northern Hemisphere or forming Tharsis. Models with several exothermic phase reactions at lower pressure and a free-slip upper boundary condition also result in a single upwelling (*Breuer et al.*, 1998). However, *Roberts and Zhong* (2006) show that the introduction of temperature- and pressure-dependent viscosity into such models increases the timescale for the development of degree-one convection to be greater

than the age of the solar system, suggesting that such phase changes cannot drive degree-one convection in Mars.

In this work I investigate whether degree-one mantle convection in Mars could result in volcanism throughout the Northern Hemisphere in the Early Hesperian. To do so I utilize finite element models of thermal convection and implement a melting rule to track the melt fraction, depth, and timing of melting. The model uses a mantle with a stratified viscosity to induce degree-one convection (*Zhong and Zuber*, 2001) and create melting in only one hemisphere. Tracking the melting variables allows for the comparison of model results with geological and petrological evidence from Mars and evaluation of the validity of my hypothesis. I evaluate the effects of initial conditions, core-mantle boundary conditions, and crustal thickness on my model to understand its robustness. By investigating the Early Hesperian resurfacing of the Northern Hemisphere, my project aims to improve our understanding of Martian thermal history and the "large-scale" puzzle of the surface age dichotomy.

Chapter 2

Methods

2.1 Model setup

I utilize the CITCOM numerical model (*Moresi and Solomatov*, 1995; *Zhong et al.*, 2000) in a spherical axisymmetric geometry (*Roberts and Zhong*, 2004) to investigate the hypothesis that degree-one convection in Mars' interior led to volcanic resurfacing of the Northern Hemisphere in the Early Hesperian. CITCOM uses the finite element method (*Hughes*, 2000) to solve the equations for thermal convection in an incompressible, infinite Prandtl number fluid under the Boussinesq approximation. In the model, thermal convection is described by the non-dimensionalized equations of conservation of mass, momentum, and energy:

$$\nabla \cdot \mathbf{u} = 0 \tag{2.1}$$

$$-\nabla P + \nabla \cdot \tilde{\boldsymbol{\tau}} = Ra\, T\, \hat{r} \tag{2.2}$$

$$\frac{DT}{Dt} = \nabla^2 T + H(t) - \rho L \frac{Df}{Dt} \tag{2.3}$$

The variables in these equations and the following paragraphs are defined in table A. The temperature is cast into potential temperature space to account for adiabatic heating. The Rayleigh number is defined as $\frac{\rho g \alpha \Delta T R_0^3}{\eta \kappa}$, using R_0^3 rather than the more common D^3 to allow for clearer non-dimensionalization in the spherical axisymmetric

geometry. The momentum equation (2.2) allows for spatially variable viscosity structure; time is non-dimensionalized by the diffusion timescale: $t^* = t\frac{\kappa}{R_0^2}$. The $\rho L\frac{Df}{Dt}$ term in the energy equation (2.3) accounts for temperature changes due to melting (see section 2.2), and $H(t)$ includes the time-dependent internal heating expected from the decay of radioactive nuclides in the interior of terrestrial planets. Decay is parameterized as in *Turcotte and Schubert* (2002) based on an initial uranium concentration, and the internal heating number is non-dimensionalized as $H^* = \frac{HR_0^2}{\rho C_p \Delta T \kappa}$.

The spherical axisymmetric geometry includes important effects of spherical geometry while significantly reducing the computational cost from fully three-dimensional models, allowing investigation of a wider range of parameters. *Roberts and Zhong* (2006) found that degree-one convection always develops more easily in three-dimensional models than in two-dimensional models, so my use of two-dimensional models is conservative regarding the development of degree-one convection. CITCOM uses a multigrid algorithm to improve the speed of solution of the momentum equation and a standard Petrov-Galerkin scheme to solve the energy equation (*Moresi and Solomatov*, 1995). The equations are solved on a grid that is 256 elements in the polar direction and 64 elements in the radial direction. The grids are refined near the top and bottom to better resolve the thermal boundary layers and near the poles to improve the solutions near these edges (Figure B-1). Test of computations with twice as many elements in both directions achieve similar results but have much longer run times. Runs utilizing the SCAM program used by *Zhong and Zuber* (2001) also have similar results. The top and bottom boundaries have free-slip boundary conditions in the polar direction and no-slip conditions in the radial direction, while the poles have the opposite. Constant temperature boundary conditions are applied at the top and bottom of the model domain to simulate a hot core-mantle boundary and a cold surface, and the poles have insulating boundary conditions for temperature. I treat the mantle as a linear viscous fluid (*Davies*, 1999) with a viscosity jump separating the upper and lower mantles, and add a stagnant lid with very high viscosity. Experiments suggest that overall, linear viscosity represents well the flow behavior of pure olivine (often used as a proxy for a more complex mantle composition) at the

temperatures and pressures of the mantle (see, e.g., *Hirth and Kohlstedt* (1995)). The models, beginning from a variety of initial conditions (see 3.2), are run for 1-2 Ga to investigate the timing of the onset of degree-one flow and melting in the Northern Hemisphere.

2.2 Melting implementation

I add a single-phase batch melting model to the flow equations to investigate the effects of melting during degree-one convection, specifically the extent and timing of melting. In this single-phase batch melting model, melting begins as the temperature of the upwelling mantle surpasses that of the solidus. From this depth to the depth where the temperature drops below the solidus, the temperature is constrained to be equal to the solidus, mimicking the temperature structure that arises in single-phase decompression melting. The melt travels with the mantle residue until the upwelling mantle reaches the conductive lid at the top of the mantle; there the temperature drops below the solidus. At this depth the melt leaves the residue and is advected immediately to the surface; this depth will be referred to as the *depth of melt segregation.* The effect of the melting rule on the temperature structure of an upwelling is illustrated in Figure B-2, which shows temperature profiles from two runs with identical initial conditions, one with melting and one without. The melt fraction f depends on the temperature difference between the bottom of the melting zone and the depth of melt segregation as well as the specific heat and heat of fusion: $f = \frac{\rho C_p \Delta T}{L}$. Decompression melting drives much of the volcanism on Earth, most significantly that associated with the creation of oceanic crust at mid-ocean ridges (*Klein and Langmuir*, 1987; *McKenzie and Bickle*, 1988) but also at many hotspots. *Monders et al.* (2006) find that the Gusev Crater basalt composition measured by the MER rover (*Gellert et al.*, 2004; *McSween et al.*, 2004) is in multiple saturation with a mantle peridotite at a depth of 85 km and a temperature of 1583 K. In addition, *Dalton et al.* (2005) propose that the Yamato 980459 meteorite may represent a direct melt of the Martian mantle, and that multiple saturation occurs around $1.2\,GPa$ and

1833K, around the same depth as *Monders et al.* (2006) (though hotter). These near-direct melts suggest that a batch melting model reasonably represents some melting processes on Mars.

2.3 Radial velocity at poles with CITCOM

Investigation of degree-one convection with CITCOM has revealed an error in the radial component of the velocity at the polar nodes. Comparing the analytic solution to Stokes flow from a Legendre polynomial buoyancy force at a single depth with the numerical result from CITCOM, I find that the polar velocity and dynamic topography agree very well. The numerical radial velocity, however, is significantly lower than the analytic value on the polar node, as shown in Figure B-3. Increasing the resolution around the pole reduces the error, but it is still noticeable. This discovery is an outcome of the investigation of behavior around the pole during degree-one convection.

Although the error in radial velocity occurs only at the pole, it likely affects the investigation of the melting due to degree-one convection. Many runs have a period with a strongly localized downwelling at the normally upwelling pole. I hypothesize that the large viscosity variations in my layered viscosity model increase the error, and that the resulting low velocity results in the growth of the thermal boundary layer to a point where it becomes unstable, causing a downwelling. While this downwelling does not seem to affect the large-scale convective planform, it does affect the local upwelling and thus the location of melting in latitude. Increasing the resolution to a level at which this error does not result in a downwelling is not feasible given current computational resources. Tests of the effects of the viscosity variations on the error in radial velocity at the pole have not yet been attempted due to time constraints. As a result, any conclusions drawn regarding the spatial distribution of melting from this study are preliminary and may be changed; additional work must be done to better understand this error in CITCOM.

Chapter 3

Model parameters and variation

3.1 The nominal model

I begin using a "nominal model" with the same parameters as *Zhong and Zuber* (2001) (table A), a set shown to result in degree-one convection. From this model I investigate the effects of variations in temperature initial conditions, core-mantle boundary properties, and crustal thickness. Rather than attempting to explore all of parameter space, I focus on understanding the physics involved and the levels and directions of dependence on important variables.

The nominal model has a layered viscosity structure with a lid of $80\,km$ thickness 500 times more viscous than the lower mantle, a 500 times less viscous upper mantle down to $750\,km$ depth, and a lower mantle with viscosity of $5 * 10^{21}\,Pas$; the viscosity is constant within each layer (*Zhong and Zuber*, 2001). The initial temperature condition is an adiabat of $1433\,K$, discussed further in section 3.2, and other parameters can be found in table A.

The melting rule I incorporate into the energy equation requires a parameterization of the solidus of a mantle of Mars composition. Moment of inertia constraints and Martian meteorite compositions have been used to estimate Martian mantle composition (*Longhi et al.* (1992); see *McSween et al.* (2003) for a more recent review). Most recently, the Mars Exploration Rover (MER) mission has returned information regarding the Martian surface composition from in-situ measurements (*Gellert et al.*,

2004; *McSween et al.*, 2004). Constraints from moment of inertia measurements are inherently non-unique; early estimates also suffer from significant measurement uncertainty (*Bills*, 1989). The best estimate of Martian mantle composition uses element ratios from Martian meteorites found on Earth (*Dreibus and Wanke*, 1985). I parameterize the solidus of *Schmerr et al.* (2001), which is based on petrological studies of the *Dreibus and Wanke* (1985) composition at pressures up to the expected Martian core-mantle boundary.

3.2 Variations from the nominal model

To understand the parameters which are important to melting induced by degree-one convection, I vary the initial temperature structure, core size, core-mantle boundary temperature, and high-viscosity lid thickness. A list of all the runs and variables relevant to these variations can be found in table A. The most fundamental and poorly constrained of these is the thermal structure of Mars at the onset of convection. The accretion of planetesimals, core segregation, and early convection at sub-mantle lengthscales all affect the initial thermal state, and none leave unambiguous signals of this state. As such, it is important for proponents of degree-one convection in Mars to demonstrate that degree-one convection arises out of most reasonable initial thermal structures. To ascertain this independence, I investigate runs with initial conditions of adiabatic gradients of temperature, conductive profiles, and typical convective structures from isoviscous runs which do not include melting. Following the work of *Elkins-Tanton et al.* (2005), I use an approximation to the temperature profile expected after the overturn of a magma ocean as an initial condition. Finally, I hypothesize that an accreting mantle might be on the verge of melting and therefore use the temperature profile of a solidus as an initial temperature condition. This set of initial temperature conditions spans the range of initial temperatures from the hottest Mars could have been at the onset of convection to the coldest. It is not exhaustive, but provides a good sampling of possible structures to assure that no structures impede degree-one convection. In all runs that lack inherent horizontal

variations the initial temperature condition is seeded with gaussian-distributed noise of less than $1K$. All cases except the convective initial conditions have a conductive lid of the same thickness as the very-high viscosity lid; the steady-state convective cases inherently contain a conductive thermal boundary layer. The average temperature profiles for all initial temperature conditions are shown in Figure B-4.

The best constraints on Martian core size come from modeling the solar tidal bulge of Mars as a function of interior structure and fitting these models to the tracking data of the Mars Global Surveyor mission. Using this method, *Yoder et al.* (2003) suggest that Mars' outer core may be liquid and has a radius of $1500\,km$ to $1850\,km$. I vary the core radius in my model, R_{CMB}, over a similar range to see the effect of lower mantle thickness on the development of degree-one convection. Measurements that show the Martian core is currently liquid also imply that the temperature of the core-mantle boundary has been at or above the liquidus since formation (*Longhi et al.*, 1992). I increase the temperature at the core-mantle boundary, T_{CMB}, from the nominal value of $1880\,K$ to $2000\,K$ at the nominal R_{CMB} of $1650\,km$ to simulate the model core composition with 14.5 weight percent S at its liquidus (*Longhi et al.*, 1992). Depending on its composition, the liquidus of the core might be even hotter, so runs with yet higher T_{CMB} would be interesting to explore. The current solidus model reaches about $2000\,K$ at a depth of $1650\,km$, so a hotter T_{CMB} results in persistent deep melting; while the complexities of such melting are an interesting area of study, they are not the focus of this work.

The thickness of the thermal boundary layer has important effects on both heat release and melting in Mars. Melting by decompression along an adiabat must occur beneath this layer, where the mantle is participating in convection. The thickness of the thermal boundary layer in the finite element model runs is largely controlled by the high-viscosity lid at the top. In ocean basins on Earth, the transition between convecting mantle and conductive thermal boundary layer occurs at about $1200\,K$. To determine the depth of this transition on early Mars, I use estimates of the lithospheric temperature gradients in the Noachian which vary from 5 to $20\,K/km$ (*McGovern et al.*, 2002). *McGovern et al.* (2002) use admittance studies to estimate

effective elastic thickness, and then apply the method of *McNutt* (1984) scaled to Mars (*Solomon and Head*, 1990) to transform these into temperature gradient. To examine how this parameter affects degree-one convection and melting, I vary the thickness of the high-viscosity lid from 50 to 110 km; while this does not explore the effects of very thick thermal boundary layers, an understanding of the effects of thickening the thermal boundary layer allows for extrapolation to such cases.

Chapter 4

Results and discussion

4.1 Results overview

My model of thermal convection with batch melting tracks the temperature and velocity fields, the melt fraction, and the depth at which melting occurs as a function of time and location. I construct movies of the evolution of temperature and velocity, melt distribution, and total melt over time (a snapshot of one of these movies is shown in Figure B-5); this allows me to examine the effects of the varied parameters on the flow structure and melting characteristics as a function of time. I compare the melt fraction, depth of melting (Figure B-6), and onset time of degree-one convection to geological and petrological evidence from Mars to validate the results. Measures of these values are discussed in the text and shown in table A.

In a total of 24 model runs, I find that degree-one convection is a common though not inevitable occurrence. All runs have a preference for low-degree convection, but in some cases the power in the flow field is split between several low-degree harmonics, while others have nearly all the power in degree-1 (see Figure B-7). Degree-one convection typically begins after 150-300 Ma, depending upon the initial temperature condition (this is discussed further in 4.2); runs with degree-one convection have average melt fractions of 15-25% and melting depths typically range from $85-200km$. Most melting after the onset of degree-one convection is distributed through only one hemisphere, and melting typically ceases by 1.5 Ga.

4.1.1 Initial thermal structure variations

I compute model runs using the following initial temperature conditions: adiabatic potential temperatures of $1333\,K$, $1433\,K$, and $1533\,K$; a conductive profile with and without internal heating; a typical isoviscous convective planform; a solidus; and an approximation of the post-overturn profile of *Elkins-Tanton et al.* (2003). The runs that begin with a temperature profile near or greater than the solidus experience significant melting in the first timesteps, and this loss of heat pushes them towards a more typical convective profile at a temperature below the solidus. I ignore this early melting as it would correspond to a very early planet-wide melting event, unrelated to the Early Hesperian resurfacing. A lull in melting sometimes occurs between the initial planet-wide melting and melting associated with the upwelling of a degree-one flow, making it easy to separate the two processes. In a few cases, however, the two overlap, resulting in unreasonably large melting depths; such runs should be viewed cautiously. Melting due to the degree-one flow commences with development of this strong upwelling. All models show a preference for low-wavelength convection, although there is often significant power in degree-two as well as degree-one; runs with inherent horizontal variations in the initial temperature conditions and conductive profiles as initial temperature conditions sometimes show significant power in higher harmonics. Runs of the nominal model varying only the random perturbation result in both pure degree-one and partly degree-two convective structures (figure B-7), indicating that the precise convective structure is dependent on small perturbations. Approximately one in three of the runs examined resulted in pure degree-one convection, although this is not formally tested. Degree-one convection seems to evolve more easily with a hotter lower mantle; initiating many runs with the same initial conditions but different perturbations shows that the $1333\,K$ adiabat and post-overturn profile initial conditions require the most attempts to initiate pure degree-one convection. Overall, the preference for long-wavelength convection in a Martian mantle with layered viscosity is strong and degree-one flow is likely, although further examination of the effects of long-lengthscale temperature perturbations would be interesting.

In addition to showing the existence of degree-one convection, investigating the initial thermal structure provides an analysis of the effects of the initial heat in the mantle. I measure the onset of degree-one convection both by the peak in the degree-one variance of mid-mantle flow and by visual inspection of the temperature and velocity fields. The spectral peak typically occurs first, but the flow has not yet achieved a stable structure at this time. I cite the visual inspection timings because they provide the time for the establishment of a stable degree-one convective flow. In general, the hotter the initial mantle the stronger the driving force, so degree-one flow develops more rapidly. The solidus initial temperature condition runs achieve degree-one convective structure faster than the post-overturn runs because the low-temperature in the lower mantle for the post-overturn runs does not provide much buoyancy. The adiabatic runs show an increase in degree-one development time with decreasing temperature. Conductive initial conditions develop degree-one convective flow very quickly, within 30 Ma, but do not sustain the structure for very long, developing a hot lower thermal boundary layer which initiates local plumes. In such runs the pre-existing thermal gradient with a lower mantle much hotter than the upper mantle may lead to large buoyancy differences, accelerating the evolution of degree-one flow. Runs with inherent horizontal temperature variations as an initial condition, such as those from isoviscous convective states, have a much longer wavelength and larger amplitude of perturbation than those with the gaussian perturbation applied. These runs develop long-wavelength convection more slowly, perhaps because the preexisting temperature perturbation must be smoothed before low-degree flow develops.

4.1.2 Core-mantle boundary radius and temperature variations

I vary R_{CMB} from 1500 to 1800 km following *Yoder et al.* (2003). The change in this value has only a small effect on the development time of degree-one convection and on melting. Figure B-8 demonstrates the lack of effect on flow pattern, showing runs

at each of the three R_{CMB} investigated at approximately the same time with very similar flow patterns. The planform of the convective flow is mostly independent of the thickness of the high-viscosity lower mantle within reasonable ranges for Martian core radii. A thinner lower mantle does lead to slightly deeper melting and thus a slightly higher melt fraction in these runs. The constant-temperature core-mantle boundary may enable slightly hotter upwellings when it is shallower, leading to larger melt fractions.

Runs with the T_{CMB} value increased to $2000\,K$ investigate the effect of increasing the core-mantle boundary temperature. The increase in bottom-temperature reduces the evolution time of degree-one convection and results in more melting over a longer period. The hotter bottom boundary provides a continuous source of additional heat; this results in hotter upwelling material and thus a larger melt fraction, as well as a slightly hotter mantle.

4.1.3 High-viscosity lid thickness variations

I vary the thickness of the high-viscosity lid from $50 - 110\ km$ to investigate the effects of variations in the top thermal boundary layer thickness. A thinner thermal boundary layer results in a larger melt fraction but a smaller melt volume. The melt fraction increases because of the larger temperature difference between the adiabatic upwelling temperatures and the solidus. A thinner thermal boundary layer cools the mantle more efficiently; this cooling more than counteracts the increased melt fraction, leading to smaller volumes of melting.

4.2 Discussion and implications

My model consistently results in degree-one convection with a melting region in one hemisphere, although the onset time of degree-one convection and various melt measures vary with the examined parameters. Runs show a strong preference for low-degree convection but the selection of pure degree-one vs mixed degree-one and degree-two convection seems to be a function of the perturbation in the initial thermal state.

Degree-one convection develops in runs both with and without the early planetwide melting, showing that this process does not drive the development of degree-one convection. The mixed low-degree convective planforms may be driven by the axisymmetric geometry; in such cases, upwelling develop on opposite sides of a downwelling and move toward the poles. The poles stop the upwellings, but in a three-dimensional geometry the upwellings might continue until they merge, forming a degree-one flow pattern. The development of both pure degree-one and mixed degree-two and degree-one flow is shown in figure B-9. I discover that long-wavelength structure develops for a wide range of possible initial temperature conditions. *Roberts and Zhong* (2006) find that degree-one convection always evolves more easily in three-dimensional models than in two-dimensions. Taken together, this suggests that if Mars has a weak upper mantle, as expected from our knowledge of rock rheology (*Karato and Wu*, 1993) and from Earth's low-viscosity upper mantle (*Hager and Richards*, 1989; *Simons and Hager*, 1997), degree-one convection is a good candidate explanation for the degree-one asymmetry of Mars.

The evolution of degree-one convective flow requires between 150 Ma and 300 Ma, and degree-one structure generally lasts for more than 1.5 Ga; most model runs do not cease degree-one convection. The quick development and loss of degree-one convective flow in conductive initial temperature conditions is anomolous, and not worrisome because it is unlikely that this initial temperature condition corresponds with ancient Mars. The onset of degree-one flow occurs slightly earlier than expected for the Early Hesperian resurfacing of the Northern Hemisphere, but is sensitive to the initial amount of heat in the mantle, the temperature of the core-mantle boundary, and the wavelength of temperature variation. *Zhong and Zuber* (2001) find that a model with temperature- and pressure-dependent viscosity requires about 400 Ma to establish degree-one convection, closer to the timing suggested by Martian geology; however, *Roberts and Zhong* (2006) suggest that degree-one flow develops in as little as 100 Ma, which is difficult to reconcile with the Early Hesperian resurfacing age. The observations do not prohibit continual volcanism from the Noachian into the Early Hesperian, they merely require that craters accumulate in numbers consistent

with an Noachian age and then be covered, and that the last major volcanism be of Hesperian age.

Melting continues until the end of the runs. The slowdown in melting is calculated by determining the time at which 90% of the total melt volume for the run (excluding early planetwide melting) has occurred. Melting typically reaches 90% completion by 1Ga, later than the Early Noachian age of the Northern Hemisphere Plains (*Tanaka et al.*, 1992; *Frey et al.*, 2002), but the late stages of melting create smaller melt fractions which might not have sufficient buoyancy to reach the surface. Mantle depletion from earlier melting will also limit later volcanism.

Martian meteorites found on Earth, and spectra from orbiting spacecraft and surface rovers, inform estimates of the composition of Mars' crust and thus provide constraints on the chemistry and petrology of Martian volcanic processes (*Longhi et al.*, 1992; *McSween et al.*, 2003; *Bandfield et al.*, 2000; *Gellert et al.*, 2004; *McSween et al.*, 2004). Typical Martian surfaces are believed to be basaltic to andesitic in composition (*Bandfield et al.*, 2000), with possible weathering in the Northern Hemisphere (*Wyatt and McSween*, 2002; *Bibring et al.*, 2005). Most Martian meteorites do not represent a melt that was in equilibrium with a primitive Martian mantle; as a result, their melting depth and melt fraction are difficult to determine. *Dalton et al.* (2005) claim that Yamato 980459, an olivine-phyric basaltic shergottite, represents a direct melt of the Martian mantle. Their experiments indicate that it separated from the mantle source at 100 km. In addition, *Monders et al.* (2006) provide a depth constraint for melting in Gusev Crater of 85 km, though the processes that dominated here may or may not be the same that operated in the Northern Hemisphere. The work of *Bertka and Holloway* (1994) implies that the Gusev Crater composition corresponds to a melt fraction of 20% from a primitive Martian mantle. The thickness of the high-viscosity lid and the upwelling temperature control the depth of melting and melt fraction in my model. A thin crustal lid brings melt segregation nearer the surface and so increases the melt fraction. A hotter upwelling mantle also increases the melt fraction; the depth of melt segregation remains about constant for this case because the high-viscosity layer, not the mantle temperature, controls this depth. In such a

case, the deeper initiation of melting increases the melt fraction. Average melt fraction in my model typically ranges from 10% to 30%, similar to the values suggested by experiments (*Bertka and Holloway*, 1994). Individual elements do achieve melt fractions up to 50% but they are rare. Melting occurs over depths of about 85 km to 200 km on average, in agreement with the petrological evidence. It is important to note that the models have not been tuned to obtain the correct value.

As noted in section 2.3, the error in radial velocity at the pole makes evaluation of the distribution of melting suspect; I will only generalize here. In runs with pure degree-one flow, melting occurs over the upwelling and so mostly in one hemisphere. The mantle does not melt solely at the pole, however, but also along the bottom of the thermal boundary layer as it flows away from the pole; it is uncertain what portion of this distant melting is due to the error in radial velocity. The distribution of volcanic thickness obtained is strongly peaked directly above the pole; this is not in agreement with the widespread volcanic plains of Mars' Northern Hemisphere. Instead, it might better model the point source of Tharsis. Once the radial velocity error is overcome, a more formal analysis of melting as a function of latitude should be undertaken. In addition, *Roberts and Zhong* (2006) show that the single upwelling of degree-one convection in three-dimensional models is not a simple cylindrical feature. The three-dimensional nature of convection might therefore significantly affect volcanic distribution. Finally, outside of a few large volcanic provinces, the source of volcanic materials in the Northern Hemisphere is unknown, so caution in analyzing melt distribution is warranted.

The thickness of the lower mantle beneath a constant thickness upper mantle has a minimal effect on the flow. A thinner lower mantle does increase the depth of melting and thus melt fraction, though the effect is small. A larger core-mantle boundary temperature, in contrast, significantly heats the mantle; this speeds the development of degree-one convection and increases the melt fraction, though within the range suggested by petrological evidence. Since the model uses a constant-temperature boundary condition, it can heat the mantle for infinite time. Future projects should investigate the interaction between a cooling core and mantle convection.

The single-phase batch melting rule in this model is thermally self-consistent and coherently implemented; it is, however, a simplification of real melting processes. Many melting processes on Earth are polybaric and near-fractional, shown by the lack of a multiple saturation of surface products with a peridotite mantle (*Klein and Langmuir*, 1987). However, these processes occur at a much smaller scale than this model, so the batch melting rule is a good compromise.

Chapter 5

Future work and conclusion

5.1 Future work

This work shows that resurfacing of the Martian Northern Hemisphere from volcanic processes driven by degree-one convection is consistent with much of the geological evidence, given the assumptions in the model. Work remains to fix the error in radial velocity at the pole in CITCOM and investigate the distribution of melting more quantitatively. Extending the investigation into three-dimensional finite-element codes will eliminate problems at the pole and allow for azimuthal variations, though at the expense of computational resources.

Other parameters affect the flow pattern and melting in finite element models, and are not well known for Martian conditions; investigation of these parameters would make the model more robust. I use a stratified viscosity for this study, but the rheology of rocks depends strongly on pressure and temperature (*Karato and Wu*, 1993). Including a temperature- and pressure-dependent viscosity would be a useful addition to this model. In addition to being a a function of temperature and pressure, the rheology of rocks depends strongly on water content (see e.g., *Karato and Wu* (1993)). *Hauck and Phillips* (2002) suggest that Mars mantle must be wet to form the crust in a time consistent with the geological evidence; this conflicts with the view of some petrologists who claim that Martian meteorites are dry (*Jones*, 1989). This debate may in part be one of semantics, as only $40\,ppm$ are necessary to achieve

the crustal growth suggested by *Hauck and Phillips* (2002). The inclusion of wet rheologies in this model could help to understand whether the viscosity differences created by water affect the development of degree-one convection. Wet rheologies add an additional complexity, as water reduces the solidus of typical mantle compositions and results in more siliceous melts (*Médard and Grove*, 2006). The partitioning of radioactive elements between mantle and crust affected the Martian thermal history significantly (*Hauck and Phillips*, 2002; *Parmentier and Zuber*, 2005) and likely influenced the timing and distribution of melting; examining the consequences of such partitioning would be an exciting avenue for future study. Investigating the effects of asymmetric boundary conditions to mimic the different crustal thicknesses of Mars in the Northern and Southern Hemispheres would also be intriguing.

The processes of convection and melting are more complex than the mathematics implemented in this and other models. Density differences in the mantle drive convection; such differences come about from variations in temperature, composition, and mineralogical phase. In this model, I consider only thermal density variations. The addition of melt buoyancy would create a model that more closely mimics the physics of a melting mantle. The chemical component of buoyancy has been investigated (*Tackley*, 2000; *Hansen and Yuen*, 2000), and found to have significant effects on convective systems. In particular for Mars, *Elkins-Tanton et al.* (2005) suggest that after magma ocean overturn the Martian mantle will have a compositional structure with high-density material in the lower mantle. This high-density material will impede convection and have a significant effect on convective structure. A melting rule that is a function of composition in addition to temperature and pressure would also make the calculation more realistic. Phase changes have been included in previous models examining degree-one convection on Mars (*Harder and Christensen*, 1996; *Breuer et al.*, 1998), and their inclusion makes any model more complete. However, *Roberts and Zhong* (2006) find that the phase changes have a small effect when included with a more realistic rheology, so the importance of a complete model will need to be weighed against the cost in computational resources.

5.2 Conclusion

The dichotomy between the Northern and Southern hemispheres on Mars in several physical properties remains an intriguing puzzle, but my hypothesis that the young age of the Northern Hemisphere could be due to volcanic resurfacing driven by degree-one convection seems consistent with much of the geological evidence. To investigate the validity of this hypothesis, I use a finite element model in a spherical axisymmetric geometry, and include a low-viscosity upper mantle. I add melting to the model to examine the resulting melt fraction and depth of melting, which I compare with geological and petrological evidence. The numerical models show a strong preference for low-degree convection, with degree-one flow as a common outcome. The melt fraction and depth are consistent with our knowledge of Martian petrology (*McSween et al.*, 2003; *Monders et al.*, 2006); though the melting is more localized than the Northern Plains would suggest, melting does occur mostly in one hemisphere. I do not rigorously investigate the distribution of melting because it is affected by an error in radial velocity around the polar node. Work examining the effects of chemistry and three-dimensional geometry will be useful to further develop and test this hypothesis. This work has important implications for the thermal and resurfacing history of Mars and other terrestrial planets.

Appendix A

Tables

Variable	Name	Definition	Value in nominal model
$\mathbf{u}$	Velocity		
P	Pressure		
$\widetilde{\tau}$	Deviatoric stress	$\eta(\nabla\mathbf{u} + \nabla^T\mathbf{u})$	
Ra	Rayleigh number	$\frac{\rho g \alpha \Delta T R_0^3}{\eta\kappa}$	$3.937 * 10^6$
ρ	Density		$3400\, kg/m^3$
g	Gravity		$3.72\, m/s^2$
α	Thermal expansivity		$3 * 10^{-5}\, 1/K$
η	Viscosity		
κ	Thermal diffusivity		$1 * 10^{-6}\, m^2/s$
t	Time		
T	Temperature		
T_0	Surface T		$273\, K$
T_{CMB}	Real T at core-mantle boundary		$1880\, K$
ΔT	Potential temperature difference between surface and core-mantle boundary	$T_{CMB} - T_0$	$1320\, K$
R_0	Mars radius		$3400\, km$
R_{CMB}	Radius of core-mantle boundary		$1650\, km$
D	Depth of mantle	$R_0 - R_{CMB}$	$1750\, km$
H	Internal heating		
C_U^0	Initial Uranium concentration		$25.7 * 10^{-9}\, kg/kg$
L	Heat of fusion		$415\, J/kg$
C_p	Specific heat of mantle		$1176\, J/kg * K$
f	Melt fraction		

Table A.1: Variables involved in the equations for thermal convection and input values for nominal model; temperatures are in potential-temperature space.

Run	Initial condition	Perturbation [1]	Ra	R_{CMB} $[km]$	T_{CMB} $[K]$	z_{lid} $[km]$	t_{total} $[Ma]$
1	Adiabat of 1433 K with conductive lid	Gaussian	$3.937 * 10^6$	1650	1880	80	1520
2	Adiabat of 1433 K with conductive lid	Gaussian	$3.937 * 10^6$	1650	1880	80	1380
3	Adiabat of 1333 K with conductive lid	Gaussian	$3.937 * 10^6$	1650	1880	80	1220
4	Adiabat of 1533 K with conductive lid	Gaussian	$3.937 * 10^6$	1650	1880	80	1580
5	Conductive with no internal heating	Gaussian	$3.937 * 10^6$	1650	1880	80	1120
6	Conduction with internal heating to make average T of 1433 K	Gaussian	$3.937 * 10^6$	1650	1880	80	1390
7	Estimate of post-overturn profile from *Elkins-Tanton et al.* (2003)	Gaussian	$3.937 * 10^6$	1650	1880	80	1480
8	Steady-state convective planform with T average about 1433 K	Inherent	$3.937 * 10^6$	1650	1880	80	1450
9	Estimate of solidus from *Schmerr et al.* (2001)	Gaussian	$3.937 * 10^6$	1650	1880	80	1500
10	Adiabat of 1433 K with conductive lid	Gaussian	$3.937 * 10^6$	1500	1880	80	1460
11	Adiabat of 1433 K with conductive lid	Gaussian	$3.937 * 10^6$	1800	1880	80	1370
12	Estimate of post-overturn profile from *Elkins-Tanton et al.* (2003)	Gaussian	$3.937 * 10^6$	1500	1880	80	1610
13	Estimate of post-overturn profile from *Elkins-Tanton et al.* (2003)	Gaussian	$3.937 * 10^6$	1800	1880	80	1370
14	Estimate of solidus from *Schmerr et al.* (2001)	Gaussian	$3.937 * 10^6$	1500	1880	80	1450
15	Estimate of solidus from *Schmerr et al.* (2001)	Gaussian	$3.937 * 10^6$	1800	1880	80	1140
16	Adiabat of 1433 K with conductive lid	Gaussian	$4.361 * 10^6$	1650	2000	80	1070
17	Estimate of post-overturn profile from *Elkins-Tanton et al.* (2003)	Gaussian	$4.361 * 10^6$	1650	2000	80	1190
18	Estimate of solidus from *Schmerr et al.* (2001)	Gaussian	$4.361 * 10^6$	1650	2000	80	1200
19	Adiabat of 1433 K with conductive lid	Gaussian	$3.937 * 10^6$	1650	1880	50	1160
20	Adiabat of 1433 K with conductive lid	Gaussian	$3.937 * 10^6$	1650	1880	110	2310
21	Estimate of post-overturn profile from *Elkins-Tanton et al.* (2003)	Gaussian	$3.937 * 10^6$	1650	1880	50	1170
22	Estimate of post-overturn profile from *Elkins-Tanton et al.* (2003)	Gaussian	$3.937 * 10^6$	1650	1880	110	2660
23	Estimate of solidus from *Schmerr et al.* (2001)	Gaussian	$3.937 * 10^6$	1650	1880	50	1160
24	Estimate of solidus from *Schmerr et al.* (2001)	Gaussian	$3.937 * 10^6$	1650	1880	110	1870

Table A.2: List of runs and the variables which are germane to the variations examined in this study.

Run	Degree-one or low-degree [2]	$t_{onset,vis}$ $[Ma]$ [3]	$t_{onset,spect}$ $[Ma]$ [4]	t_{90} $[Ma]$ [5]	$< f >$ [6]	$z_{melt,max}$ $[km]$ [7]	$z_{melt,min}$ $[km]$ [8]
1	Degree-one	204	158	1140	15.3%	211	84
2	Low-degree	217	167	1080	15.1%	211	84
3	Low-degree	192	178	1120	16.1%	190	84
4	Degree-one	179	130	1060	15.9%	233	84
5	Degree-one	31	27	1070	15.6%	169	84
6	Degree-one	37	16	1330	21.7%	318	84
7	Degree-one	148	42	996	16.5%	254	84
8	Low-degree	338	256	1120	14.6%	211	84
9	Degree-one	118	85	950	18.0%	817	84
10	Degree-one	203	162	1130	14.5%	191	84
11	Degree-one	205	169	1080	16.0%	211	84
12	Degree-one	168	45	1030	15.3%	212	84
13	Degree-one	125	59	919	17.5%	254	84
14	Degree-one	101	78	870	18.8%	972	84
15	Low-degree	119	86	808	19.4%	1480	84
16	Low-degree	182	172	931	18.4%	296	84
17	Degree-one	108	36	888	18.8%	403	84
18	Degree-one	111	84	866	19.2%	849	84
19	Low-degree	190	152	918	19.5%	190	63
20	Degree-one	289	214	1590	13.7%	233	126
21	Degree-one	103	39	719	19.3%	339	63
22	Degree-one	312	113	1570	14.4%	254	126
23	Degree-one	93	64	682	18.7%	403	63
24	Degree-one	177	129	1300	16.4%	849	126

Table A.3: List of runs and the results in terms of degree-one convection and melting, melt fraction, and melt depth.

[1]Gaussian perturbation to initial temperature profile or planform with inherent horizontal variation

[2]Pure degree-one or mixed degree-one and degree-two (low-degree) flow

[3]t of stable degree-one or low-degree onset, visual

[4]t of degree-one or low-degree onset, spectra

[5]t of 90% melt

[6]Average melt fraction

[7]Maximum depth of melting

[8]Minimum depth of melt segregation

Appendix B

Figures

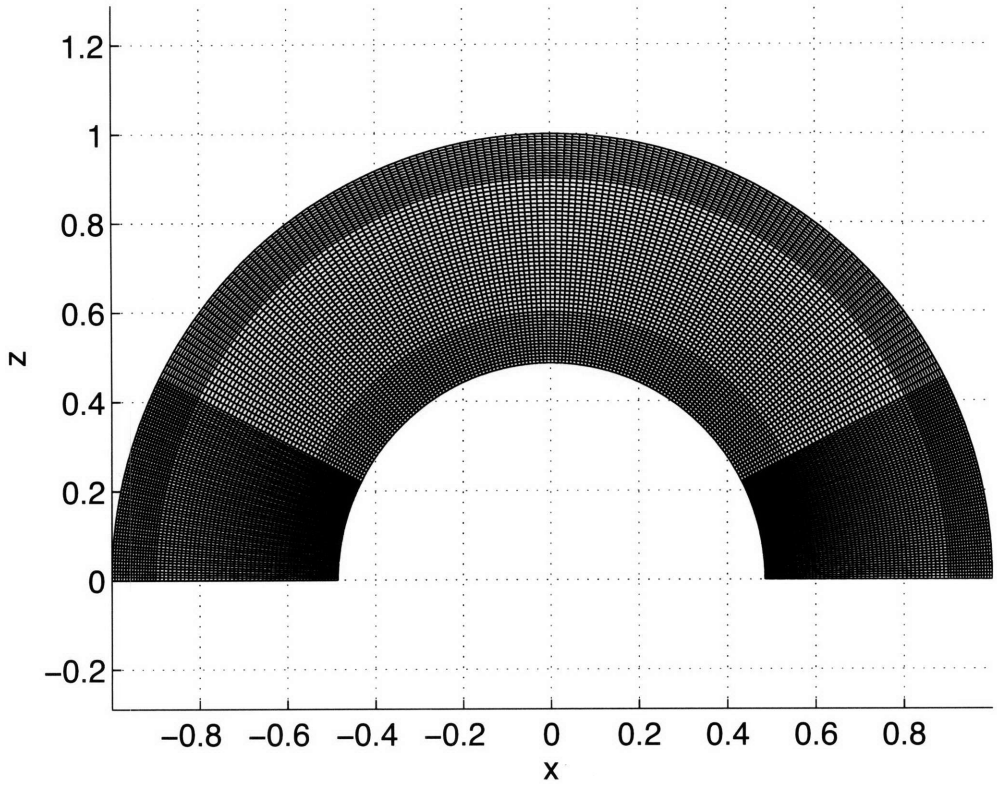

Figure B-1: Plot of the grid on which the finite element model is run; it has 64 elements in the radial direction and 256 elements in the latitudinal direction.

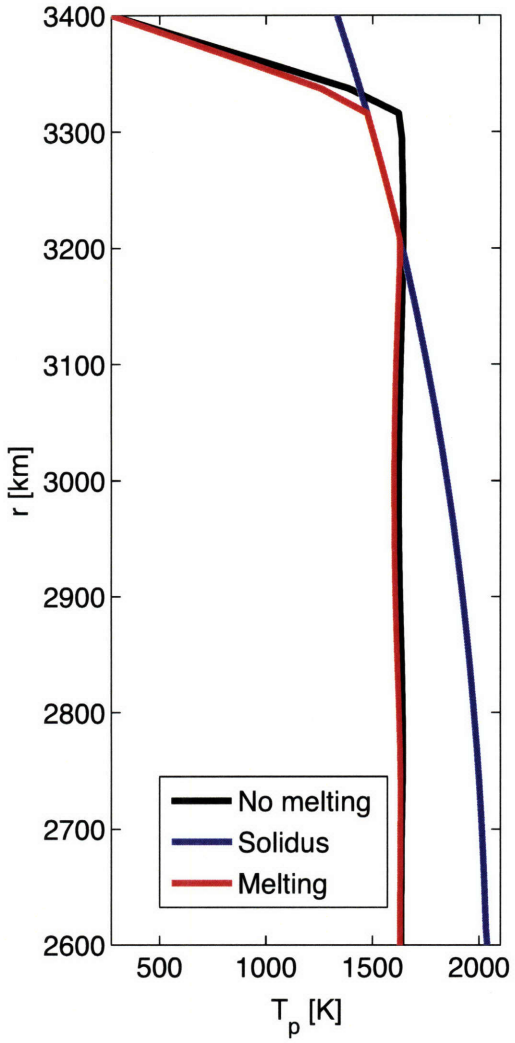

Figure B-2: Typical temperature profiles for upwelling mantle in finite element models. T_p is potential temperature, and r is radius in km. The profile without melting is calculated in a run with identical initial conditions and model parameters as the one with melting, except that the melting model is turned off. The initial temperature condition in these runs is a 1433 K adiabat beneath the conducting lid, seeded with gaussian-distributed noise. The solidus is from *Schmerr et al.* (2001). Note that the temperature in the run with melting never exceeds the solidus.

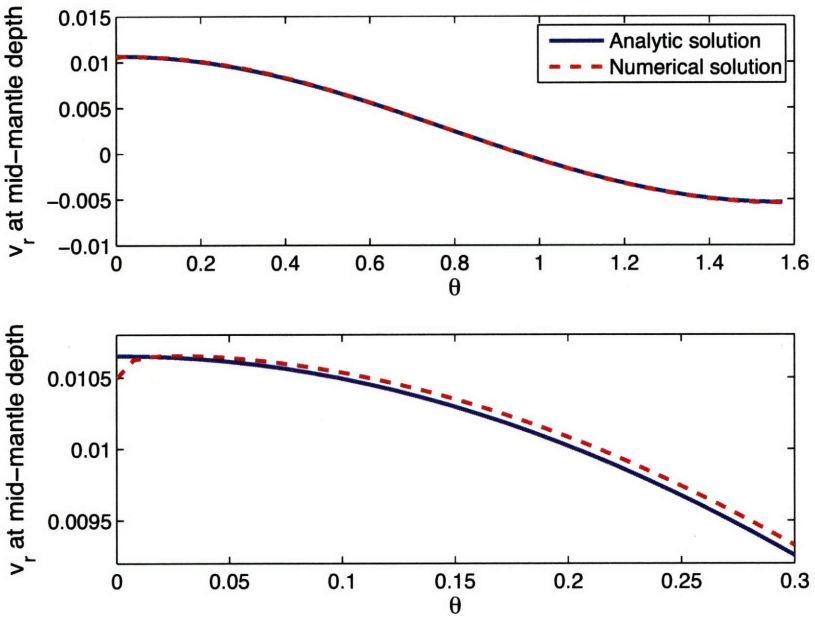

Figure B-3: Plots of the radial velocity given by analytic solution to a Legendre polynomial buoyancy force at a single depth (equally spaced solution points given by *Zhong* (2006)), and the numerical solutions given by CITCOM for the grid used in this project. The upper plot shows the generally good agreement between the analytic and numerical solutions; the lower plot zooms in on the pole and shows the misfit right at the pole.

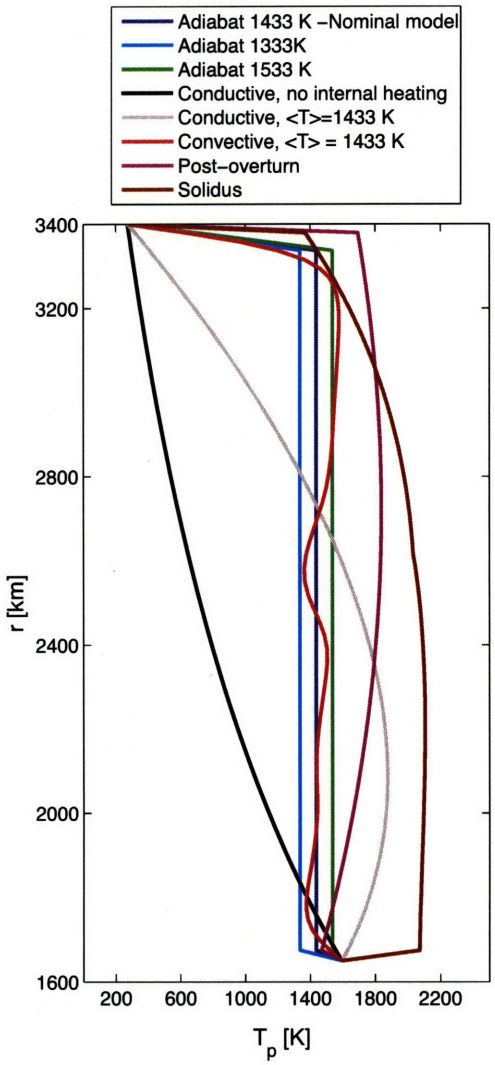

Figure B-4: Horizontally-averaged profiles of the initial temperature conditions examined in this study, with the bottom boundary enforced. See section 3.2 for description of these temperature profiles. The adiabatic, conductive, post-overturn, and solidus temperature fields have been seeded with gaussian noise. The convective profile inherently includes horizontal temperature variations. T_p is potential temperature, and r is radius in km. The solidus initial condition is hotter than the core-mantle boundary at the beginning of the model run, but cools quickly.

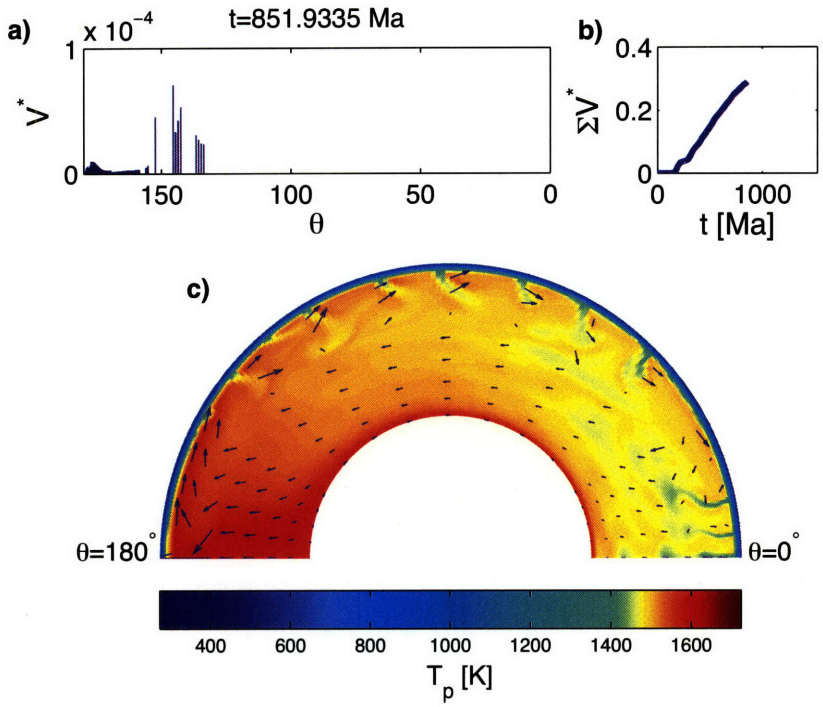

Figure B-5: Frame from a movie displaying the time evolution of thermal convection and melting results after 850 Ma. a) is a plot of non-dimensional melt volume (V^*) vs θ, and has been oriented in the same direction as c). V^* is in non-dimensional units and is actually the volume over a small-circle of the given latitude, as appropriate for the spherical-axisymmetric geometry. b) is a plot of the total melt volume over all latitudes vs. time. c) is a plot showing the temperature and velocity fields for a model timestep. T_p is potential temperature in K, as specified by the color legend; the size of arrows corresponds to magnitude of velocity. This run uses an initial temperature condition of an adiabat at 1433 K and the nominal parameters.

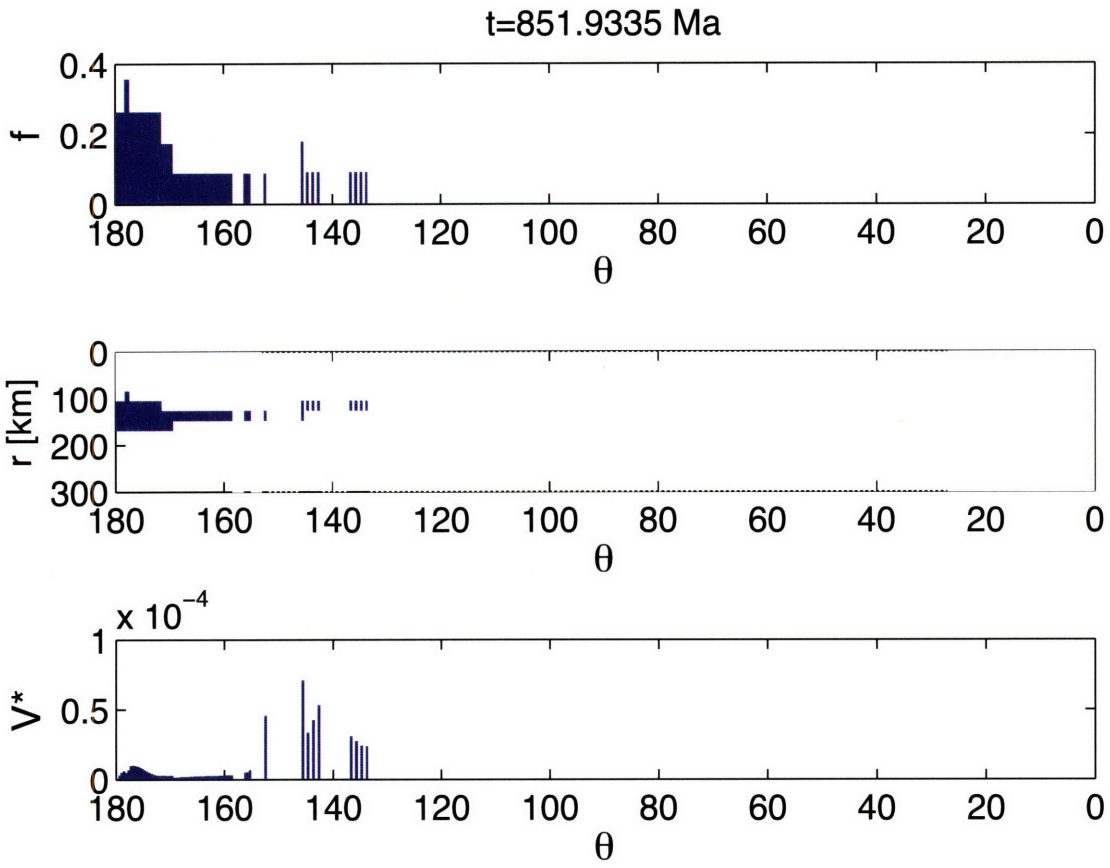

Figure B-6: Melt fraction f, melt zone, and melt volume as a function of latitude for the same step as figure B-5. a) shows the melt fraction; steps are due to grid resolution. b) shows the depths where melting occurs as shaded regions. c) shows the non-dimensional volume of melt in the same manner as a).

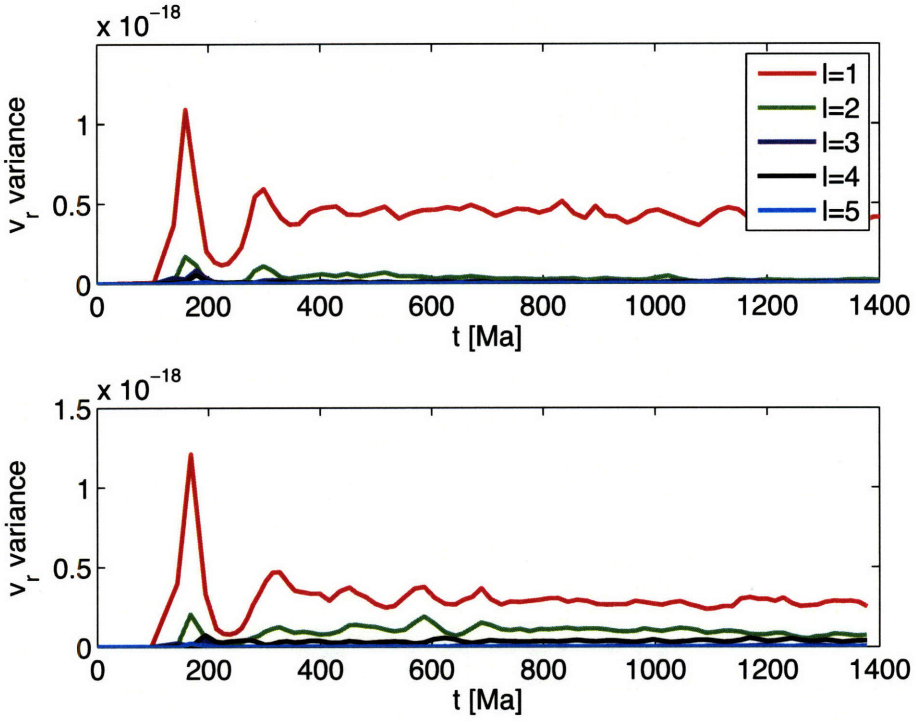

Figure B-7: Spectrum of the radial velocity field at mid-mantle depth for runs with the nominal model but different gaussian noise perturbations. Note that the upper run has nearly all the power in the degree-one term after the large spike, while the lower run has significant variance in the degree-two and degree-four terms. Since the only difference is the perturbation, the precise convective planform is a function of the perturbation.

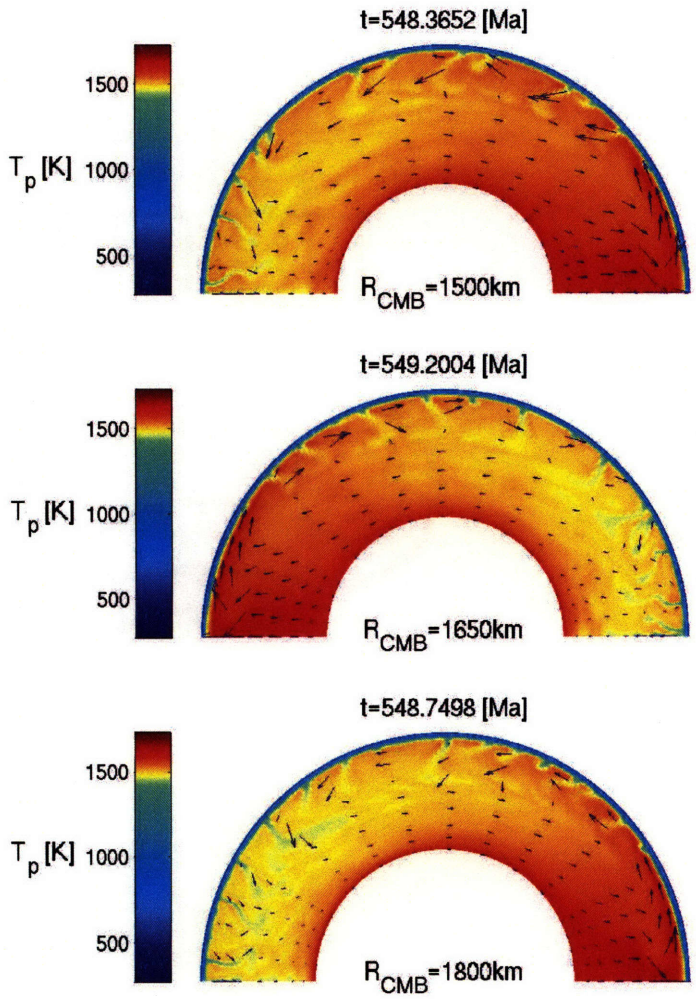

Figure B-8: Potential temperature and velocity fields for runs with three different values of R_{CMB}, as listed in the figure, with all other parameters held constant. Temperature is shown in color, as specified in the color maps (K). The size of the arrows indicates the magnitude of velocity. Note that the structures are very similar, suggesting that the R_{CMB} is not important to the behavior of the system. The direction of degree-one convection is an effect of the gaussian noise imposed as an initial perturbation.

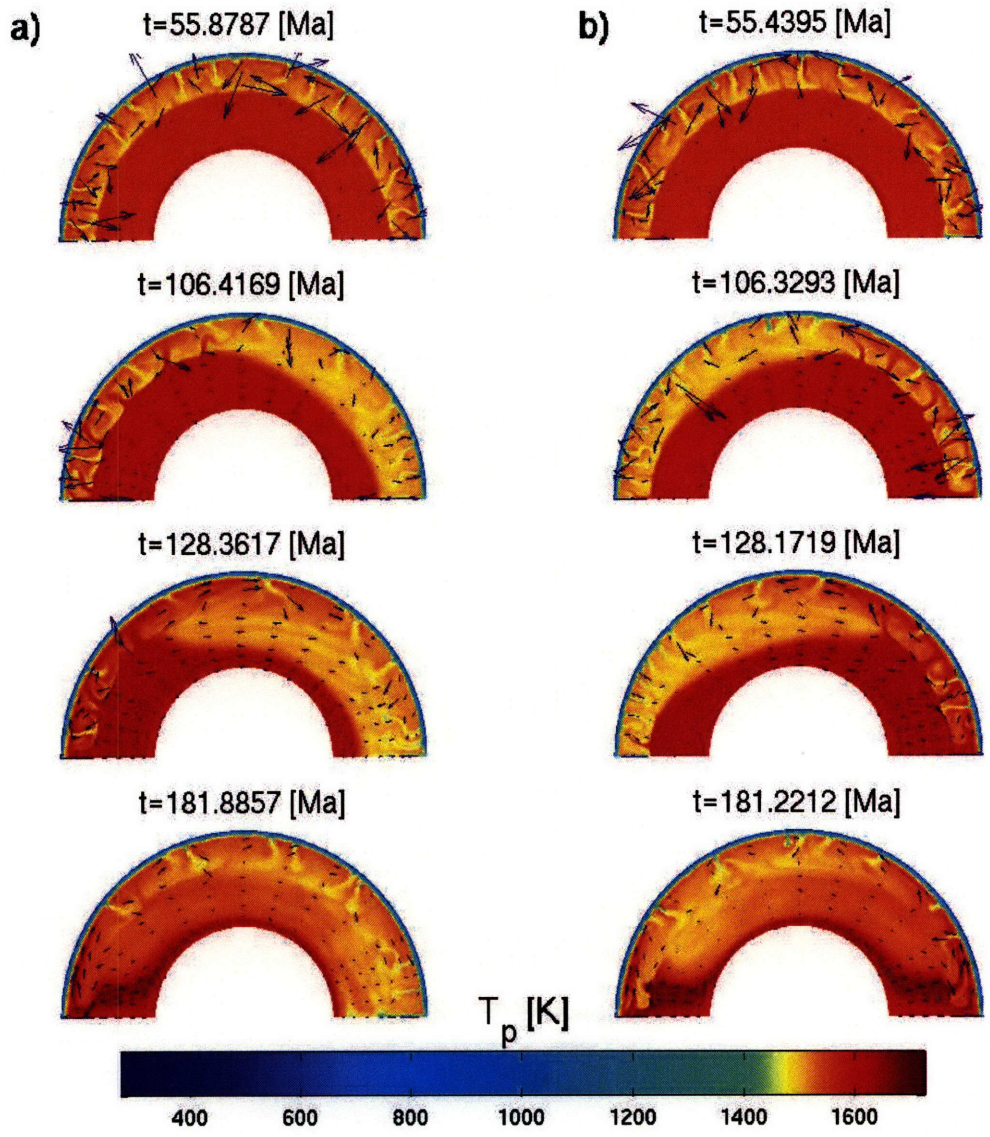

Figure B-9: Time evolution of pure degree-one (a) and mixed degree-one and degree-two (b) convective flow for a run with identical initial conditions and parameters except for the gaussian perturbation. The initial temperature condition is an adiabat of 1533 K. Note how the mixed degree-one and degree-two structure has an initial downwelling in the middle of the mantle and the upwellings split, getting stuck at the poles.

Bibliography

Bandfield, J., V. Hamilton, and P. Christensen (2000), A Global View of Martian Surface Compositions from MGS-TES, *Nature*, *287*, 1626–1630.

Bertka, C., and J. Holloway (1994), Anhydrous partial melting of an iron-rich mantle II: primary melt compositions at 15 kbar, *Contrib. Mineral Petrol.*, *115*, 313–322.

Bibring, J.-P., Y. Langevin, A. Gendrin, B. Gondet, F. Poulet, M. Berthe, A. Soufflot, R. Arvidson, N. Mangold, J. Mustard, P. Drossart, and the OMEGA team (2005), Mars surface diversity as revealed by the omega/mars express observations, *Science*, *307*, 1576–1581.

Bills, B. (1989), The moments of inertia of Mars, *Geophys. Res. Let.*, *16*(5), 385–388.

Breuer, D., D. Yuen, T. Spohn, and S. Zhang (1998), Three dimensional models of Martian mantle convection with phase transitions, *Gephys. Res. Let.*, *25*(3), 229–232.

Carr, M., and J. I. Head (2003), Oceans on Mars: An assessment of the observational evidence and possible fate, *J. Geophys. Res.*, *108*(E5), doi:10.1029/2002JE001963.

Connerney, J., M. Acuna, P. Wasilewski, N. Ness, H. Reme, C. Mazelle, D. Vignes, R. Lin, D. Mitchell, and P. Cloutier (1999), Magnetic Lineations in the Ancient Crust of Mars, *Science*, *284*, 794–798.

Connerney, J., M. Acuna, N. Ness, G. Kletetschka, D. Mitchell, and H. Reme (2005), Tectonic implications of Mars crustal magnetism, *Pro. Nat. Acad. Sci.*, *102*(42), 14,970–14,975, doi:10.1073/pnas.0507469102.

Dalton, H., D. Musselwhite, W. Kiefer, and A. Treiman (2005), Experimental petrology of the basaltic Shergotitte Yamato 980459: Implications for the thermal structure of the Martian mantle, in *Lunar and Planetary Science Conf. XXXVI*, 2142.pdf.

Davies, G. (1999), *Dynamic Earth*, Cambridge University Press, The Edinburgh Building, Cambridge CB2 2RU, UK.

Dreibus, G., and H. Wanke (1985), Mars, a volatile-rich planet, *Meteoritics*, *20*(2), 367–381.

Elkins-Tanton, L., S. Zaranek, E. Parmentier, and P. Hess (2005), Early magnetic field and magmatic activity on Mars from magma ocean cumulate overturn, *Earth and Planet. Sci. Let.*, *236*, 1–12, doi:10.1016/j.epsl.2005.04.044.

Elkins-Tanton, L. T., E. Parmentier, and P. Hess (2003), Magma ocean fractional crystallization and cumulate overturn in terrestrial planets: Implications for Mars, *Meteor. and Planet. Sci.*, *38*(12), 1753–1771.

Esposito, P., W. Banerdt, G. Lindal, W. Sjogren, M. Slade, B. Bills, D. Smith, and G. Balmino (1992), *Mars*, chap. Gravity and Topography, The University of Arizona Press.

Frey, H., J. Roark, K. Shockey, E. Frey, and S. Sakimoto (2002), Ancient lowlands on Mars, *Geophys. Res. Let.*, *29*(10), doi:10.1029/2001GL013832.

Gellert, R., R. Rieder, R. Anderson, J. Brückner, B. Clark, G. Dreibus, T. Economou, G. Klingelhöfer, G. Lugmair, D. Ming, S. Squyres, C. d'Uston, H. Wänke, A. Yen, and J. Zipfel (2004), Chemistry of the Rocks and Soils in Gusev Crater from the Alpha Particle X-ray Spectrometer, *Science*, *305*, 829–832.

Greeley, R., and J. Guest (1987), Geologic map of the eastern equatorial region of Mars, U.S. Geol. Srv. Misc. Invest.Map.

Hager, B., and M. Richards (1989), Long-wavelength variations in Earth's geoid: Physical models and dynamical implications, *Phil. Trans. R. Soc. Lond. Ser. A*, *328*, 309–327.

Hansen, U., and D. Yuen (2000), Extended-Boussinesq thermal-chemical convection with moving heat sources and variable viscosity, *Earth and Planetary Science Letters*, *176*, 401–411.

Harder, H., and U. Christensen (1996), A one-plume model of martian mantle convection, *Nature*, *380*, 507–509.

Hartmann, W. (1973), Martian Cratering, 4, Mariner 9 Initial Analysis of Cratering Chronology, *J. Geophys. Res.*, *78*(20), 4096–4116.

Hauck, S. I., and R. Phillips (2002), Thermal and crustal evolution of Mars, *J. Geophys. Res.*, *107*(E7), doi:10.1029/2001JE001801.

Head, J. I., H. Hiesinger, M. Ivanov, M. Kreslavsky, S. Pratt, and B. Thomson (1999), Possible Ancient Oceans on Mars: Evidence from Mars Orbiter Laser Altimeter Data, *Science*, *286*, 2134–2137.

Head, J. I., M. Kreslavsky, and S. Pratt (2002), Northern Lowlands of Mars: Evidence for widespread volcanic flooding and tectonic deformation in the Hesperian Period, *J. Geophys. Res.*, *107*(E1), doi:10.1029/2000JE001445.

Hirth, G., and D. Kohlstedt (1995), Experimental constraints on the dynamics of the partially molten upper mantle: Deformation in the diffusion creep regime, *J. Geophys. Res.*, *100*(B2), 1981–2001.

Hughes, T. (2000), *The finite element method: linear static and dynamic finite element analysis*, 2nd ed., Dover, 31 East 2nd St., Mineola, N.Y. 11501.

Hynek, B., and R. Phillips (2001), Evidence for extensive denudation of the Martian Highlands, *Geology*, *29*(5), 407–410.

Jones, J. (1989), Isotopic relationships among the shergottites, the nakhlites and chassigny, in *Pro. of the 19th Lunar and Planet. Sci. Conf.*, pp. 465–474.

Karato, S., and P. Wu (1993), Rheology of the Upper Mantle: A Synthesis, *Science*, *260*, 771–778.

Klein, E., and C. Langmuir (1987), Global Correlations of Ocean Ridge Basalt Chemistry with Axial Depth and Crustal Thickness, *J. Geophys. Res.*, *92*(B8), 8089–8115.

Kreslavsky, M., and J. Head. (2000), Kilometer-scale roughness of Mars' surface: Results from MOLA data analysis, *J. Geophsy. Res.*, *105*, 26,695–26,712.

Longhi, J., E. Knittle, J. Holloway, and H. Wanke (1992), *Mars*, chap. The bulk composition, mineralogy, and internal structure of Mars, pp. 184–208, The University of Arizona Press.

McGovern, P., S. Solomon, D. Smith, M. Zuber, M. Simons, M. Wieczorek, R. Phillips, G. Neumann, O. Aharonson, and J. Head (2002), Localized gravity/topography admittance and correlation spectra on Mars: Implications for regional and global evolution, *J. Geophys. Res.*, *107*(E12), doi: 10.1029/2002JE001854.

McKenzie, D., and M. Bickle (1988), The Volume and Composition of Melt Generated by Extenstion of the Lithosphere, *Journal of Petrology*, *29*(3), 625–679.

McNutt, M. (1984), Lithospheric flexure and thermal anomalies, *J. Geophys. Res.*, *89*(B13), 11,180–11,194.

McSween, H., R. Arvidson, J. I. Bell, D. Blaney, N. Cabrol, P. Christensen, B. Clark, J. Crisp, L. Crumpler, D. Des Marais, J. Farmer, R. Gellert, A. Ghosh, S. Gorevan, T. Graff, J. Grant, L. Haskin, K. Herkhenhoff, J. Johnson, B. Jolliff, G. Klingelhoefer, A. Knudson, S. McLennan, K. Milam, J. Moersch, R. Morris, R. Rieder, S. Ruff, P. J. deSouza, S. Squyres, H. Wänke, A. Wang, M. Wyatt, A. Yen, and

J. Zipfel (2004), Basaltic Rocks Analyzed by the Spirit Rover in Gusev Crater, *Science*, *305*, 842–845.

McSween, H. J., T. Grove, and M. Wyatt (2003), Constraints on the composition and petrogenesis of Mars, *J. Geophys. Res.*, *108*(E12), doi:10.1029/2003JE002175.

Médard, E., and T. Grove (2006), Early hydrous melting and degassing of the martian interior: an experimental study, *J. Geophys. Res.*, in press.

Monders, A., E. Médard, and T. Grove (2006), Basaltic lavas at Gusev Crater revisited, in *Lunar and Planetary Science Conf. XXXVII*, 1834.pdf.

Moresi, L.-N., and V. Solomatov (1995), Numerical investigation of 2D convection with extremely large viscosity variations, *Phys. Fluids*, *7*(9), 2154–2162.

Mustard, J., F. Poulet, A. Gendrin, J.-P. Bibring, Y. Langevin, B. Gondet, N. Mangold, G. Bellucci, and F. Altieri (2005), Olivine and pyroxene diversity in the crust of mars, *Science*, *307*, 1594–1597.

Neumann, G., M. Zuber, M. Wieczorek, P. McGovern, F. Lemoine, and D. Smith (2004), Crustal structure of Mars from gravity and topography, *J. Geophys. Res.*, *109*, doi:10.1029/2004JE002262.

Parker, T., R. Saunders, and D. Schneeberger (1989), Transitional morphology in Deuteronilus Mensae, Mars: Implications for modification of the lowland/upland boundary, *Icarus*, *82*(1), 111–145.

Parmentier, E., and M. Zuber (2005), Tales concerning the early evolution of Mars, a story told in equations and numbers, In Preparation.

Phillips, R., M. Zuber, S. Solomon, M. Golombek, B. Jakosky, W. Banerdt, D. Smith, R. Williams, B. Hynek, O. Aharonson, and S. I. Hauck (2001), Ancient Geodynamics and Global-Scale Hydrology on Mars, *Science*, *291*, 2587–2591.

Roberts, J., and S. Zhong (2004), Plume-induced topography and geoid anomalies and their implications for the Tharsis rise on Mars, *J. Geophys. Res.*, *109*, doi: 10.1029/2003JE002226.

Roberts, J., and S. Zhong (2006), Degree-1 convection in the Martian mantle and the origin of the hemispheric dichotomy, *J. Geophys. Res.*, *111*(E06013), doi: 10.1029/2005JE002668.

Schmerr, C., Y. Fei, and C. Bertka (2001), Extending the solidus for a model iron-rich Martian mantle composition, in *Lunar and Planet. Science Conf. XXXII*, 1157.

Scott, D., and K. Tanaka (1986), Geologic map of the western equatorial region of Mars, U.S. Geol. Surv. Misc. Invest.Map.

Simons, M., and B. Hager (1997), Localization of the gravity field and the signature of glacial rebound, *Nature*, *390*, 500–504.

Sleep, N. (1994), Martian plate tectonics, *J. Geophys. Res.*, *99*(E3), 5639–5655.

Smith, D., M. Zuber, S. Solomon, R. Phillips, J. Head, J. Garvin, W. Banerdt, D. Muhleman, G. Pettengill, G. Neumann, F. Lemoine, J. Abshire, O. Aharonson, C. Brown, S. Hauck, A. Ivanon, P. McGovern, H. Zwally, and T. Duxbury (1999), The Global Topography of Mars and Implications for Surface Evolution, *Science*, *284*(5419), 1495–1503.

Solomon, S., and J. Head (1990), Heterogeneities in the Thickness of the Elastic Lithosphere on Mars: Constraints on Heat Flow and Internal Dynamics, *J. Geophys. Res.*, *95*(B7), 11,073–11,083.

Solomon, S., O. Aharonson, J. Aurnou, W. Banerdt, M. Carr, A. Dombard, H. Frey, M. Golombek, S. I. Hauck, J. I. Head, B. Jakosky, C. Johnson, P. McGovern, G. Neumann, R. Phillipsn, D. Smith, and M. Zuber (2005), New Perspectives on Ancient Mars, *Science*, *307*, 1214–1220.

Tackley, P. (2000), Mantle Convection and Plate Tectonics: Toward an Integrated Physical and Chemical Theory, *Science*, *288*, 2002–2007.

Tanaka, K., and D. Scott (1987), Geologic map of the polar regions of Mars, U.S. Geol. Surv. Misc. Invest.Map.

Tanaka, K., D. Scott, and R. Greeley (1992), *Mars*, chap. Global Stratigraphy, pp. 345–382, The University of Arizona Press, Tucson and London.

Tanaka, K., J. Skinner, T. Hare, T. Joyal, and A. Wenker (2003), Resurfacing history of the northern plains of Mars based on geologic mapping of Mars Global Surveyor data, *J. Geophys. Res.*, *108*(E4), doi:10.1029/2002JE001908.

Turcotte, D., and G. Schubert (2002), *Geodynamics*, Cambridge.

Wilhelms, D., and S. Squyres (1984), The martian hemispheric dichotomy may be due to a giant impact, *Nature*, *309*, 138–140.

Wyatt, M., and H. J. McSween (2002), Spectral evidence for weathered basalt as an alternative to andesite in the northern lowlands of Mars, *Nature*, *417*, 263–266.

Yoder, C., A. Konopliv, D. Yuan, E. Standish, and W. Folkner (2003), Fluid Core Size of Mars from Detection of the Solar Tide, *Science*, *300*, 299–303.

Zhong, S. (2006), personal communication, see http://anquetil.colorado.edu/szhong/XSphere.

Zhong, S., and M. Zuber (2001), Degree-1 mantle convection and the crustal dichotomy on Mars, *Earth and Planetary Sciene Letters*, *189*, 75–84.

Zhong, S., M. Zuber, L. Moresi, and M. Gurnis (2000), Role of temperature-dependent viscosity and surface plates in spherical shell models of mantle convection, *J. Geophys. Res.*, *105*(B5), 11,063–11,082.

Zuber, M., S. Solomon, R. Phillips, D. Smith, G. Tyler, O. Aharonson, G. Balmino, W. Banerdt, J. Head, C. Johnson, F. Lemoine, P. McGovern, G. Neumann, D. Rowlands, and S. Zhong (2000), Internal Structure and Early Thermal Evolution of

Mars from Mars Global Surveyor Topography and Gravity, *Science*, *287*, 1788–1793.